MATERIALS SCIENCE

Dynamics and healing behavior of metallosupramolecular polymers

Laura N. Neumann[1], Emad Oveisi[2], Albrecht Petzold[3], Robert W. Style[4], Thomas Thurn-Albrecht[3], Christoph Weder[1]*, Stephen Schrettl[1]*

Self-healing or healable polymers can recuperate their function after physical damage. This process involves diffusion of macromolecules across severed interfaces until the structure of the interphase matches that of the pristine material. However, monitoring this nanoscale process and relating it to the mechanical recovery remain elusive. We report that studying diffusion across healed interfaces and a correlation of contact time, diffusion depth, and mechanical properties is possible when two metallosupramolecular polymers assembled with different lanthanoid salts are mended. The materials used display similar properties, while the metal ions can be tracked with high spatial resolution by energy-dispersive x-ray spectrum imaging. We find that healing actual defects requires an interphase thickness in excess of 100 nm, 10 times more than previously established for self-adhesion of smooth films of glassy polymers.

INTRODUCTION

Because the possibility to heal defects in polymeric objects is of substantial technological relevance, the design of materials that enable this function and the development of a fundamental understanding of the underlying processes are of considerable interest (*1*–*5*). In thermoplastic polymers, healing of severed surfaces can be achieved by heating above the glass transition or melting temperature (*6*–*8*), and the process involves the steps of surface rearrangement, wetting, diffusion of macromolecules across the interface, chain reentanglement, and randomization (*6*). According to the reptation model, the terminal relaxation time of entangled macromolecules (T_r) is related to molecular weight M by $T_r \propto M^3$ (*9*, *10*), and healing rates consequently decrease with increasing M in a power law dependency. The ensuing problem that healing of high–molecular weight polymers is slow can be mitigated in polymers featuring covalent or noncovalent dynamic bonds (*4*, *5*, *11*). For example, the reversible association of binding motifs causes the temporary disassembly of supramolecular polymers upon exposure to suitable stimuli. The resulting decrease in the apparent molecular weight of linear polymers or the cross-link density of networks increases chain mobility and reduces viscosity (*12*), and healing processes are accelerated. When the stimulus is removed, supramolecular polymers reassemble (*4*, *5*). This approach has been exploited in a range of polymers (*2*, *3*), many of which were assembled through hydrogen bonds or metal-ligand interactions (*13*–*18*). If the interphase created by the healing process is indistinguishable from the pristine material, then the original properties can be fully restored (Fig. 1A) (*1*). Quantitative studies of such interphase formation are, however, rare. Schnell *et al.* (*19*, *20*) have shown that an interfacial width of 11 to 22 nm is required for self-adhesion in polystyrene. This was possible by combining fracture mechanics tests and neutron reflectivity experiments on nanoscale bilayers in which scattering contrast was established by using one deuterated layer. The results agree with computational and interdiffusion studies on other glassy polymers (*8*). Similar investigations with chemically more complex polymers are exceedingly difficult, and healing of polymers containing dynamic bonds is therefore typically probed by macroscopic experiments, such as the qualitative observation of the disappearance of scratches (*3*, *4*, *21*), or by comparing the mechanical properties of damaged and healed samples (*14*–*18*, *22*). For example, the recovery of the elongation at break, tensile strength, and/or toughness is established by tensile tests (*14*, *21*, *23*–*25*) or fracture mechanics (*26*–*28*). Efforts to examine healing processes on a microscopic level include in situ Raman (micro)spectroscopy (*29*, *30*), internal reflection infrared imaging (*31*, *32*), and laser speckle imaging (*33*). These studies corroborate that polymer diffusion is essential for efficient healing, but a quantification of the interphase formation is challenging, and it remains unclear what extent of diffusion is necessary to achieve complete healing in supramolecular and many other polymers.

Here, we report an approach that allows monitoring of the interphase formed upon healing actual or simulated defects with a spatial resolution of a few nanometers. The approach relies on mending two otherwise identical metallosupramolecular polymers (MSPs) that were assembled with different metal ions. The two different ion types can be distinguished in a spatially resolved manner by energy-dispersive x-ray (EDX) spectrum imaging in scanning transmission electron microscopy (STEM). This allows monitoring of their diffusion across the interface (Fig. 1B) and thereby facilitates a correlation between the contact time, the depth of the interphase, and the macroscopic mechanical properties. We find notable differences to self-adhesion in glassy polymers, including that the required interphase thickness for complete healing in MSPs and, by extension, of similar healable polymers is an order of magnitude larger.

RESULTS

Characterization of the Eu-based metallopolymer

The macromonomer used in this study was based on a rubbery, amorphous poly(ethylene-*co*-butylene) (PEB) core of a number-averaged molecular weight of 3100 g mol^{-1} that was terminated with two 2,6-bis(1′-methylbenzimidazolyl)pyridine (Mebip) ligands; this

[1]Adolphe Merkle Institute, University of Fribourg, Chemin des Verdiers 4, 1700 Fribourg, Switzerland. [2]Interdisciplinary Centre for Electron Microscopy, EPFL, 1015 Lausanne, Switzerland. [3]Naturwissenschaftliche Fakultät II–Chemie, Physik und Mathematik, Institut für Physik, Martin-Luther-Universität Halle-Wittenberg, von-Danckelmann-Platz 3, 06120 Halle (Saale), Germany. [4]Department of Materials, Soft and Living Materials, ETH Zürich, Vladimir-Prelog-Weg 10, 8093 Zürich, Switzerland. *Corresponding author. Email: christoph.weder@unifr.ch (C.W.), stephen.schrettl@unifr.ch (S.S.)

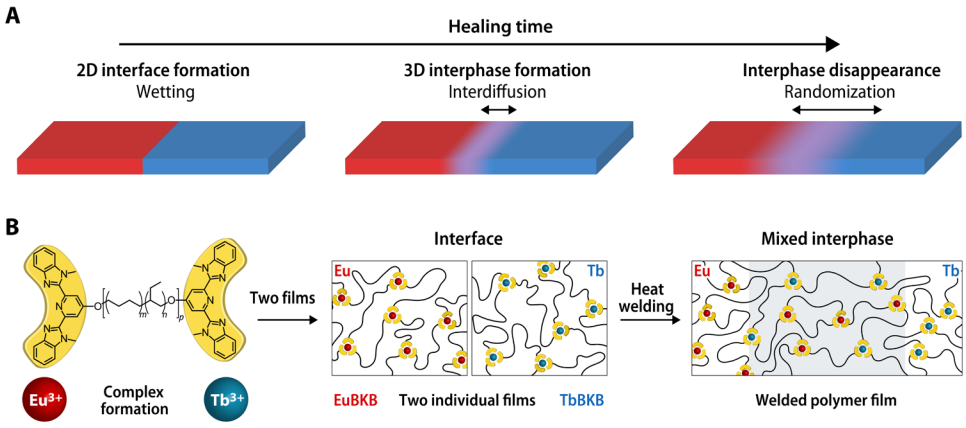

Fig. 1. The healing process in polymers. (**A**) The final stages of the healing process in polymers involve wetting, interdiffusion with reentanglement, and randomization. (**B**) To investigate the healing process on a length scale of a few nanometers, metallosupramolecular polymers (MSPs) assembled from telechelic PEB with terminal Mebip ligands (M_n = 3800 g mol^{-1}; $m \approx 0.32$, $n \approx 0.68$, $p \approx 55$) and either $Eu(ClO_4)_3$ or $Tb(ClO_4)_3$ were studied. The two metallosupramolecular polymers display similar properties, but the different ion types can be monitored in a spatially resolved manner.

building block (BKB) was previously used to create healable MSPs with metal ions such as Zn^{2+}, Fe^{2+}, La^{3+}, and Eu^{3+} (*14*, *34*–*36*). Because Mebip forms trifold coordination complexes with lanthanoid ions (*37*, *38*), BKB and such ions assemble into networks (*14*, *35*, *36*, *39*). Expecting that MSPs made from BKB and Eu^{3+} or Tb^{3+} salts display similar properties (*40*, *41*), we first investigated one of these materials in detail. Thus, 250-µm-thick homogeneous, colorless films of **EuBKB** were prepared following earlier reports (see the Supplementary Materials for details) (*35*, *42*), and the mechanical properties and microphase separation of the metal-ligand complexes and the hydrophobic polymer were ascertained by tensile tests and small-angle x-ray scattering (SAXS) (figs. S1 and S2), respectively. To establish at which temperature the dynamics of the metallosupramolecular bonds in **EuBKB** render the healing process conveniently observable (*21*, *43*), dynamic mechanical analyses (DMAs) and linear shear rheology experiments were carried out. The DMA measurements reveal a T_g at −20°C, a room temperature storage modulus E' of 14.1 ± 0.5 MPa, and a gradual decrease in E' before the samples fail at 138° ± 7°C (fig. S3). The loss tangent trace shows maxima around −20°, 70°, and 125°C, which we relate on the basis of a recent study (*36*) to the T_g of the soft phase that predominantly consists of the PEB cores (−20°C), the temperature at which individual metal-ligand complexes in the soft phase become dynamic (70°C), and the softening of the hard phase formed by the metal-ligand complexes that phase separate from the soft phase (125°C), respectively. The hard phase physically cross-links the MSP, and its softening promotes complete network relaxation (*12*, *44*). Thus, above the T_g, the mechanical properties of **EuBKB** are governed by a transient network structure with temperature-dependent dynamics. To probe this further, the effective supramolecular bond lifetime (τ_b), which corresponds to the time scale of reversible association between supramolecular moieties, was determined by linear shear rheology based on the reciprocal value of the crossover frequency of the storage and loss moduli ($\tau_b = 2\pi/\omega_{cr}$) in temperature-dependent oscillatory frequency sweeps (*45*–*47*). Master curves for **EuBKB**, established by time-temperature superposition, suggest that at 20°C, τ_b exceeds 1 year, while it decreases to ca. 200 s at 80°C, 16 s at 100°C, and fractions of seconds above 120°C (figs. S3 and S4). The value of τ_b at 80°C is within the range where dynamic supramolecular materials display efficient healing on a reasonable experimental time scale (*17*, *43*), and this temperature was therefore chosen for systematic studies of the healing process.

Healing of the Eu-based metallopolymer

Adopting a widely used protocol to simulate actual defects (*13*–*17*), rectangular strips of **EuBKB** films were freshly cut at the center, and the severed interfaces were welded at 80°C in a square butt joint geometry for 5 to 60 min. To ensure comparable results, all samples were subjected to welding within 2 min after cutting. The extent of healing was then determined by uniaxial tensile tests (figs. S5 and S6). Plots of the healing efficiencies (defined as the property ratios of pristine and cut/healed samples) against the healing time reveal that the original properties are essentially fully recovered after 10 min and that no significant changes occur for longer healing times (Fig. 2, A to C, and table S1). The healing efficiencies based on maximum strength, elongation at break, and toughness after 10 min are 96 ± 10, 87 ± 16, and 85 ± 21%, respectively. The recovery of all mechanical parameters progresses with a similar time dependence (Fig. 2, A to C). Annealing experiments confirm that the material is not altered by heating per se (fig. S7 and table S2). As expected in view of the high τ_b at ambient temperature, **EuBKB** does not self-heal well under ambient conditions; even after 15 weeks, the healing efficiency based on the recovered tensile strength (88 ± 8%), strain at break (46 ± 7%), and toughness (42 ± 10%) remains low (fig. S8).

Healing of **EuBKB** was further investigated by fracture mechanics experiments. Half of the interface of severed samples was brought into contact, while a thin spacer was placed between the other half to maintain a notch during welding at 80°C (fig. S9). Samples were then subjected to uniaxial deformation perpendicular to the notch direction, and the mechanical properties were compared to those of reference samples in which an equivalent notch had been applied by cutting. The healing efficiencies established after 10 min—94 ± 5% for the tensile strength, 110 ± 15% for the elongation at break, and 94 ± 5% for the toughness—confirm complete healing (figs. S10 and S11 and table S3). The progression of the healing process was examined on the basis of the stress intensity factor K_1, which is independent of the testing geometry and loading conditions (see Materials and Methods for details) (*48*). The recovery of K_1 (Fig. 2D) mirrors the kinetics established in the square butt joint geometry (Fig. 2, A

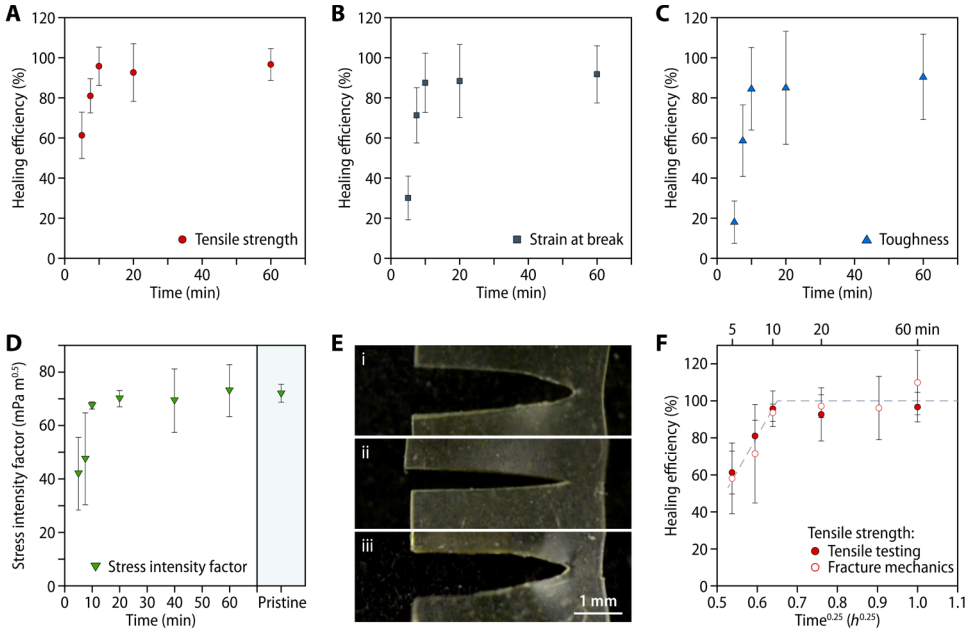

Fig. 2. Healing of EuBKB. (**A** to **C**) Plots of the healing efficiency at 80°C as a function of healing time based on the recovery of (A) tensile strength, (B) strain at break, and (C) toughness. (**D**) Plot of the stress intensity factor K_1 of EuBKB determined via fracture mechanics experiments as a function of healing time. (**E**) Photographs showing the propagating crack tip during the fracture of a notched **EuBKB** film in the (i) pristine state, (ii) after healing a severed sample for 5 min, and (iii) after complete healing (10 min). (**F**) Comparison of the tensile strength–based healing efficiency as a function of healing time ($t^{0.25}$) determined from tensile tests as well as fracture mechanics experiments. The dashed lines serve as a guide to the eye.

to C) and corroborates that the mechanical properties of **EuBKB** are fully recovered after ca. 10 min at 80°C. An inspection of samples under load shows that in partially healed samples (welded for 5 min at 80°C), the fracture progresses along the interface with a crack tip opening displacement (CTOD) at the onset of crack propagation of ca. 37 ± 10 μm (Fig. 2E and fig. S12). Fully healed samples (welded for 10 min at 80°C), however, display a CTOD at the onset of crack propagation of ca. 147 ± 23 μm, values comparable to those of pristine samples of 165 ± 24 μm, suggesting that a well-mixed interphase has formed.

Theory relates the healing efficiency to the interpenetration of chains across the interface and predicts, based on the reptation model of chain dynamics (*9*, *10*), that the recovery of the tensile strength over time t is proportional to $t^{0.25}$ (*6*, *7*, *26*). While the self-diffusive behavior in **EuBKB** samples is unlikely to proceed via reptation, the analysis of the recovery of the mechanical properties nonetheless corroborates that the hindered diffusion of the supramolecular network correlates with this relationship in the experimentally accessible timeframe of 5 to 10 min (Fig. 2F) (*49*). Moreover, the plateau regime with healing efficiencies of 100% at longer times suggests that the dynamic reconfiguration leads to the formation of a homogeneous network structure that is comparable to the one of the pristine samples, i.e., randomization occurs.

Characterization of the Tb-based metallopolymer and blends

Exploiting that MSPs based on different lanthanoid salts can display similar properties (*40*, *41*), we substituted $Eu(ClO_4)_3$ with $Tb(ClO_4)_3$ and prepared **TbBKB** films using the same process as for **EuBKB**. To determine the properties of the interphase that is formed upon welding the two different MSPs, we prepared mixed ion **(Eu/Tb)BKB** films from BKB and an equimolar mixture of $Eu(ClO_4)_3$ and $Tb(ClO_4)_3$. Our investigation of these materials paralleled that of **EuBKB** (figs. S13 to S18 and table S4). The data show that the stress strain, modulus, and loss tangent traces all mirror each other (fig. S13), with the only difference that the E' traces of **TbBKB** and **(Eu/Tb)BKB** above ca. 60°C display a steeper slope than the trace of **EuBKB**, which may reflect slight differences in either hard-phase formation or dynamics. Rheological experiments show that **TbBKB** exhibits a considerably longer τ_b than **EuBKB** ($3.0{\cdot}10^3$ s vis-à-vis 200 s at 80°C) (figs. S14 and S16), which reflects different kinetic rates for the dissociation of these complexes, despite the fact that Tb^{3+} and Eu^{3+} display comparable binding constants in solution (*40*, *50*). By contrast, the bond lifetime (τ_b) of **(Eu/Tb)BKB** at 80°C (200 s) matches the one of **EuBKB**, showing that the relaxation processes in the already randomized material are a consequence of energy dissipation through the more dynamic Eu^{3+} complexes (fig. S17).

Welding experiments demonstrate that the higher τ_b of **TbBKB** translates into slower healing in comparison to **EuBKB**. At 80°C, a healing time of ca. 40 min was required for **TbBKB** to reach healing efficiencies of 99 ± 7 (tensile strength), 88 ± 17 (elongation at break), and 88 ± 22% (toughness) (figs. S19 and S20), whereas similar values were observed for **EuBKB** after only 10 min. Welding samples of mixed **(Eu/Tb)BKB** films at 80°C revealed a healing time of 60 min, with efficiencies based on maximum strength, elongation at break, and toughness of 92 ± 23, 102 ± 9, and 91 ± 29%, respectively (figs. S21 and S22). While the different dynamics complicate the analysis of the healing kinetics, the data suggest that the process is governed by the less dynamic Tb^{3+} complexes, although relaxation processes in the mixed material are dominated by the more dynamic Eu^{3+} complexes. Thus, the mechanical properties of **(Eu/Tb)BKB** are only recovered once the Tb^{3+} complexes have rearranged and

the interphase features an entangled network with a density comparable to pristine samples.

Healing of nonsymmetric metallosupramolecular interfaces

Having established the individual healing behavior, we set out to explore the welding of the two components under formation of a mixed **EuBKB/TbBKB** interphase. In this case, defects were simulated by cutting films of the two MSPs and welding freshly cut pieces at 80°C for 5 to 120 min, and the welded samples were then subjected to uniaxial tensile tests (fig. S23). Lacking a direct reference for mixed **EuBKB/TbBKB** joints, the values for tensile strength, elongation at break, and toughness were used to monitor the progression of healing. Plots of these parameters against the healing time show that the properties plateau between 60 and 120 min of welding (Fig. 3, A to D), with a minimal but not statistically significant increase between the last two time points. The data for samples that were welded for 120 min show that the properties are on par with those of pristine materials, notably, the **(Eu/Tb)BKB** films (figs. S24 and S25), corroborating that complete healing has occurred. The kinetics suggest that the less dynamic Tb^{3+} complexes govern the process. Moreover, a plot of the tensile strength against $t^{0.25}$ indicates that healing across the mixed interface also follows the established stages of interphase formation and randomization (Fig. 3D) (*6*, *26*).

Because the two materials fluoresce in different colors (red in the case of **EuBKB** and blue-green in the case of **TbBKB**), the interface can be imaged by fluorescence microscopy (Fig. 3E and figs. S26 and S27). This was exploited to monitor crack propagation in fracture mechanics tests of notched **EuBKB/TbBKB** samples. Gratifyingly, in samples that had been healed for 120 min, the crack propagation deviates from the original interface, and a random advance of the crack into the bulk **EuBKB** or **TbBKB** fraction is discernible under ultraviolet (UV) light illumination (Fig. 3F, fig. S26, and movie S1). In accordance with these qualitative observations, the mechanical properties determined in fracture experiments match those of neat **EuBKB** and **TbBKB** (figs. S28 to S30 and table S5). A comparison with the stress-strain curve recorded upon fracture mechanics testing of notched **(Eu/Tb)BKB** corroborates that crack propagation in **EuBKB/TbBKB** samples deviates from the inherently weaker interphase into the bulk materials after 120 min of healing (fig. S29). Hence, the investigations of the healing across the interface of MSPs with different metal ions unambiguously confirm that an interphase is established and that after 120 min at 80°C, randomization occurs so that the properties of the mixed phase become barely distinguishable from those of the two parent polymers.

To probe the spatial distribution of metal ions across the interface, we analyzed the cross sections of **EuBKB/TbBKB** joints welded for various times at 80°C by STEM-EDX (Fig. 4A and figs. S31 to S33). The acquired EDX line scans with the corresponding intensities for europium and terbium across the interface were then fitted to a logistic sigmoid function, with an interphase width corresponding to the distance between the points where the fitted signal intensity is equal to 80 and 20% of the respective total intensities (Fig. 4B). As evident from the EDX maps and line scans, the migration of metal ions across the interface is symmetric with some statistical fluctuation (fig. S34), and the width of the mixed interphase featuring both europium and terbium increases with time from 29 ± 7 nm for 5 min of healing to 104 ± 35 nm after 60 min and reaches 175 ± 41 nm

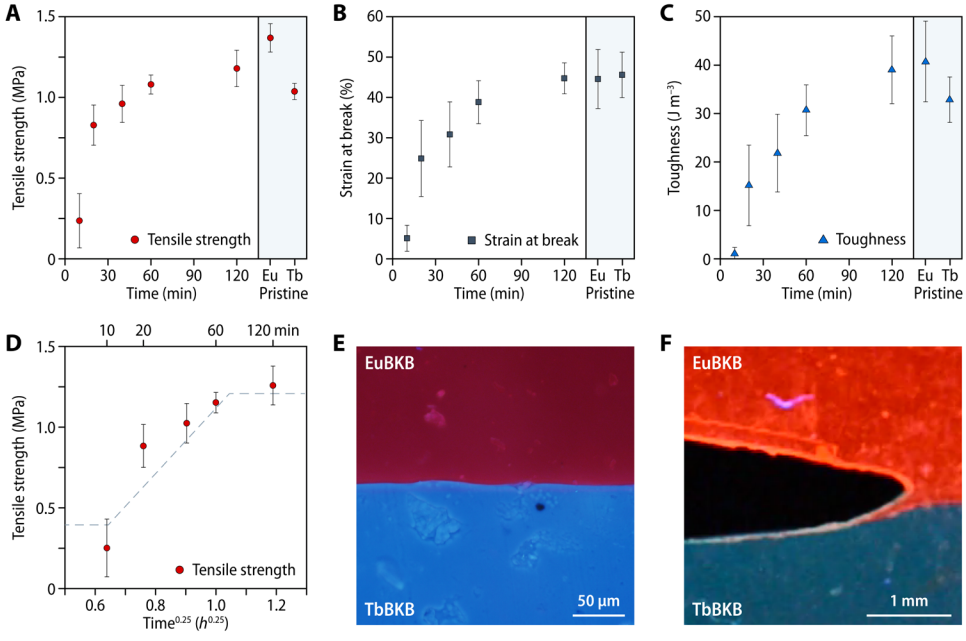

Fig. 3. Healing experiments involving the formation of a mixed EuBKB/TbBKB interphase. (**A** to **C**) Plots of the mechanical properties of welded **EuBKB/TbBKB** samples as a function of healing time at 80°C based on (A) tensile strength, (B) strain at break, and (C) toughness, as well as a comparison with the properties of pristine samples. The maximum values are reached after ca. 60 min. Since no reference values can be established for such mixed joints, the absolute mechanical properties are monitored in lieu of a healing efficiency. (**D**) Plot of the tensile strength as a function of welding time ($t^{0.25}$) as determined from tensile tests. The dashed line serves as a guide to the eye. (**E**) Fluorescence microscopy image of the interface of a healed **EuBKB/TbBKB** film. The luminescence of the different lanthanoid ions complexed with Mebip ligands renders the **EuBKB** fraction appearing red and the **TbBKB** fraction appearing bluish/green when placed under ultraviolet (UV) light illumination (λ_{ex} = 365 nm). (**F**) Photograph showing the crack tip of a notched **EuBKB/TbBKB** sample during deformation under UV light illumination (healing time = 120 min and λ_{ex} = 365 nm). The deviation of the propagating crack from the original interface corroborates complete healing.

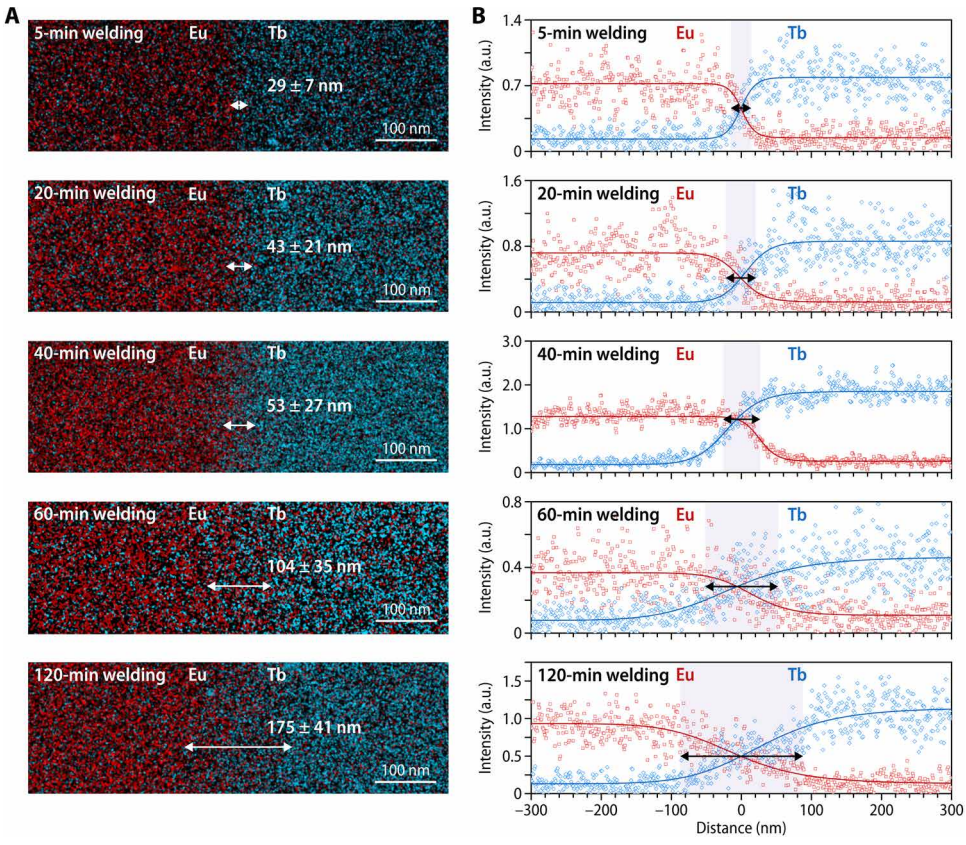

Fig. 4. Visualization of the interphase. STEM coupled with EDX was used to study the interphase of samples obtained after welding **EuBKB** and **TbBKB** films together for different amounts of time. (**A**) Representative EDX elemental maps of Eu (red) and Tb (blue) across the original interface. (**B**) Representative individual EDX line scans of the intensity of Eu-L and Tb-L lines (open symbols) across the interface and the sigmoidal logistics fit (solid line) after healing times of 5, 20, 40, 60, and 120 min (top to bottom). a.u., arbitrary units.

after 120 min, indicating that a mixed interphase of more than 100 and less than 175 nm is required to achieve complete recovery of the mechanical properties. The symmetric ion migration across the interface reflects that the dissociation of the metal-ligand complexes is thermodynamically unfavorable (*38*, *50*, *51*). While **EuBKB** is more dynamic than **TbBKB** (vide supra), the Eu^{3+} ions cannot migrate into the **TbBKB** before free ligands become available. Therefore, the diffusion across the polymer-polymer interface must be symmetric, and the less dynamic Tb^{3+} complexes limit the exchange rate. Solution binding constants (*38*) suggest that the metal ions remain coordinated to at least one but likely two Mebip ligands of the macromonomers throughout the dynamic dissociation and association processes during healing. Therefore, ion migration appears to be a reasonable indication for the rearrangement of the entire supramolecular polymer. This important relation has not been unequivocally demonstrated, but it is supported by the finding that the thickness of the observed interphases exceeds the dimensions of the spacing between hard metal-ligand and soft PEB domains (<7 nm; figs. S1, S15, and S18).

DISCUSSION

The interphase thickness required to restore the MSPs' mechanical properties is considerably higher than the 11 to 22 nm reported for the welding of glassy homopolymers (*19*, *20*). Since the latter studies involved smooth interfaces and testing in an asymmetric double cantilever beam geometry, the considerable differences may be related to the roughness of the separately cut MSP films used herein, geometric factors of the mechanical testing, the interfacial structure, and wetting kinetics. Perhaps more important, however, are the different responses of the materials to mechanical deformation. The MSPs studied here are rubbery polymer networks with barely any entanglements (M_e of PEB ca. 2000 g mol^{-1}) (*52*) in which the domains formed by metal-ligand complexes act as effective cross-linking points (*36*). The effectiveness of these cross-links for the mechanical properties of the MSPs may hence be considerably different than the entanglements of glassy, high–molecular weight polymers (typically more than 10 M_e), and more substantial interdiffusion is apparently necessary in the case of the supramolecular polymers to restore the effective cross-link density and bulk mechanical properties.

Experimental work and theoretical modeling have corroborated that high molecular mobility and efficient diffusion across polymer-polymer interfaces are the key requirements for healing, and supramolecular interactions therefore represent an attractive basis for the design of healable polymeric materials. The MSPs investigated here can be readily healed, and the efficiency and time dependence of the process correlate with the relaxation time of the metal-ligand complexes. The design of the study allowed a rare insight into how the recovery of mechanical properties relates to interphase formation. Quite unexpectedly, the interphase thickness required to achieve complete healing of cuts applied to the MSPs greatly exceeds the

previously reported values for the adhesion of flat films of glassy polymers, indicating that this parameter is not universal. Since most self-healing or healable polymers are—similar to the presently investigated materials—soft and feature reversible bonds and typical healing scenarios involve defects such as the ones studied here, our findings appear to be highly relevant. Our data show unequivocally that in this case, microscopic techniques with a resolution of the order of tens of nanometers or less may be suitable to probe the underlying process. Moreover, recent direct studies of diffusion in metal-coordinated transient polymer networks suggest complex and unexpected superdiffusive behavior that promotes polymer "hopping" rather than "walking" (*53*–*55*). Knowledge gained through such studies should be useful to develop a better understanding of the healing process and to guide the further design of new polymers with improved healing characteristics.

MATERIALS AND METHODS

Metallosupramolecular polymerization and formation of films

To a stirred solution of the BKB macromonomer in $CHCl_3$, a solution of a stoichiometric amount of the metal salt in anhydrous MeCN was added. The solution was stirred for 10 min, the solvent was removed in vacuo, and the solid residue was dissolved in $CHCl_3$. The solution was dried in vacuo and placed in a vacuum oven overnight at 40°C, and a rigid transparent material of polymeric appearance with appreciable mechanical properties was obtained. The material was processed into films of a uniform thickness of ca. 250 μm by compression molding between Kapton sheets at 100°C in a Carver CE Press with a pressure of 3 metric tons that was applied for 4 min.

Sample preparation for tensile testing

Films with a thickness of ca. 250 μm, a length of 12 mm, and a width of 4 mm were placed on a Kapton sheet, cut in the middle into two pieces, and realigned. The samples were placed between two glass slides with aluminum spacers with a thickness of ca. 200 μm and clamped. Within 2 min after cutting, the samples were welded at 80°C for the indicated time. Subsequently, samples were removed from the glass slides, cut into dog bones with a custom-made dog bone cutter, and subjected to tensile testing.

Sample preparation for fracture mechanics testing

Samples for fracture mechanics were prepared by placing a small piece of aluminum foil covering 2 mm of the freshly cut interface to prevent welding at this section and leave a notch in the welded sample. Within 2 min after cutting, the samples were placed between two glass slides with aluminum spacers with a thickness of ca. 200 μm, clamped, and welded at 80°C for the indicated time. Thereafter, samples were removed from the glass slides, the aluminum foil was carefully removed, and the samples were subjected to fracture mechanics testing. During the testing, a movie of the rupture process was recorded.

Tensile testing and fracture mechanics measurements

Both tensile testing and fracture mechanics measurements were conducted using a TA Instruments DMA Q800. Uniaxial tensile testing was carried out with dog bone–shaped pristine or welded samples prepared as described above. For fracture mechanics, testing pristine or welded samples that feature a notch to ca. 50% of the sample width were used, and the samples were subjected to uniaxial deformation perpendicular to the direction of the notch. For both tensile testing and fracture mechanics, a strain rate of 5% min^{-1}, an initial strain of 0.05%, and a preload force of 0.0 N were used. The stress intensity factor K_1 was calculated from the mechanical data determined from the stress-strain curves during fracture mechanics testing according to the following formula (*48*)

$$K_1 = \sigma\sqrt{\pi a}\left[1.12 - 0.23\left(\frac{a}{b}\right) + 10.6\left(\frac{a}{b}\right)^2 - 21.7\left(\frac{a}{b}\right)^3 + 30.4\left(\frac{a}{b}\right)^4\right] \quad (1)$$

where σ corresponds to the maximum stress, with a and b as the notch length and sample width, respectively. The prerequisites for this equation, $h/b \geq 1$ and $a/b \leq 0.6$, where h is the sample length, are met in the present case. For a comparison of the determined values for K_1 with those of other studies, one needs to take into account that the herein used experimental setup slightly deviates from the model used to derive Eq. 1. The CTOD was determined by analysis of still images during fracture mechanics testing, at the point where the crack just started to extend. We draw lines that emerge into the crack from the crack tip, at 45° to the symmetry axis of the crack. The CTOD is defined as the distance between the points where these lines intersect the crack faces.

STEM with EDX spectroscopy

Samples for STEM-EDX analysis were prepared by cryo-ultramicrotomy using a Leica EM FC7 machine that was equipped with a Diatome cryo-knife (35° angle). Microtomy was carried out at −50°C with a cutting speed of 0.2 mm s^{-1}, and ultramicrotomed sample slices were deposited on an ultrathin carbon support grid. EDX data were acquired using a Thermo Fisher Titan Themis 60-300, equipped with a high-brightness Schottky X-FEG gun, four silicon drift Super-X EDX detectors, and Velox acquisition software. A focused electron probe was scanned (raster of 1024 × 1024 pixels) across a region of interest in the STEM mode to collect EDX data in the form of spectrum images. For each scan point, the electron scattering incident on a high-angle annular dark-field detector was recorded to obtain the structural information while simultaneously obtaining an EDX spectrum by collecting the x-rays emitted from the local volume probed by the electron beam. The spectrum images were acquired with a probe current of ca. 0.6 nA, an acceleration voltage of 200 kV, and a spatial sampling of 1 nm $pixel^{-1}$ and 1.8 to 2.1 ms $pixel^{-1}$ dwell times (for a total acquisition time of ~30 min). To account for effects of surface roughness, line scans across the interface were constructed in representative sample areas that feature an approximately linear interface by integrating the intensity of the Tb-L and Eu-L peaks over a width of 100, 200, 400, or 800 pixels parallel to the interface (see data file S1, "Data line scans"). The line scans obtained via EDX were fitted to the sigmoidal logistics function

$$y = \frac{A_1 - A_2}{1 + \left(\frac{x}{x_0}\right)^p} + A_2 \quad (2)$$

and the width of the interphase was defined as the distance between the y points of 20 and 80% of the signal intensity, respectively. The reported interphase widths for the different healing times are averages determined through the evaluation of 4 to 12 independent EDX line scans (see data file S1), and all errors are SDs.

SUPPLEMENTARY MATERIALS

Supplementary material for this article is available at http://advances.sciencemag.org/cgi/content/full/7/18/eabe4154/DC1

REFERENCES AND NOTES

1. Y. Yang, M. W. Urban, Self-healing polymeric materials. *Chem. Soc. Rev.* **42**, 7446–7467 (2013).
2. L. M. de Espinosa, G. L. Fiore, C. Weder, E. Johan Foster, Y. C. Simon, Healable supramolecular polymer solids. *Prog. Polym. Sci.* **49–50**, 60–78 (2015).
3. Y. Yang, X. Ding, M. W. Urban, Chemical and physical aspects of self-healing materials. *Prog. Polym. Sci.* **49–50**, 34–59 (2015).
4. A. Campanella, D. Döhler, W. H. Binder, Self-healing in supramolecular polymers. *Macromol. Rapid Commun.* **39**, 1700739 (2018).
5. Y. Yang, M. W. Urban, Self-healing of polymers via supramolecular chemistry. *Adv. Mater. Interfaces* **5**, 1800384 (2018).
6. R. P. Wool, K. M. O'Connor, A theory crack healing in polymers. *J. Appl. Phys.* **52**, 5953–5963 (1981).
7. Y. H. Kim, R. P. Wool, A theory of healing at a polymer-polymer interface. *Macromolecules* **16**, 1115–1120 (1983).
8. R. P. Wool, Self-healing materials: A review. *Soft Matter* **4**, 400–418 (2008).
9. P. G. de Gennes, Reptation of a polymer chain in the presence of fixed obstacles. *J. Chem. Phys.* **55**, 572–579 (1971).
10. T. P. Russell, V. R. Deline, W. D. Dozier, G. P. Felcher, G. Agrawal, R. P. Wool, J. W. Mays, Direct observation of reptation at polymer interfaces. *Nature* **365**, 235–237 (1993).
11. R. J. Wojtecki, M. A. Meador, S. J. Rowan, Using the dynamic bond to access macroscopically responsive structurally dynamic polymers. *Nat. Mater.* **10**, 14–27 (2011).
12. E. B. Stukalin, L.-H. Cai, N. A. Kumar, L. Leibler, M. Rubinstein, Self-healing of unentangled polymer networks with reversible bonds. *Macromolecules* **46**, 7525–7541 (2013).
13. P. Cordier, F. Tournilhac, C. Soulié-Ziakovic, L. Leibler, Self-healing and thermoreversible rubber from supramolecular assembly. *Nature* **451**, 977–980 (2008).
14. M. Burnworth, L. Tang, J. R. Kumpfer, A. J. Duncan, F. L. Beyer, G. L. Fiore, S. J. Rowan, C. Weder, Optically healable supramolecular polymers. *Nature* **472**, 334–337 (2011).
15. Y. Chen, A. M. Kushner, G. A. Williams, Z. Guan, Multiphase design of autonomic self-healing thermoplastic elastomers. *Nat. Chem.* **4**, 467–472 (2012).
16. D. W. R. Balkenende, C. A. Monnier, G. L. Fiore, C. Weder, Optically responsive supramolecular polymer glasses. *Nat. Commun.* **7**, 10995 (2016).
17. Y. Yanagisawa, Y. Nan, K. Okuro, T. Aida, Mechanically robust, readily repairable polymers via tailored noncovalent cross-linking. *Science* **359**, 72–76 (2018).
18. B. Qin, S. Zhang, P. Sun, B. Tang, Z. Yin, X. Cao, Q. Chen, J.-F. Xu, X. Zhang, Tough and multi-recyclable cross-linked supramolecular polyureas via incorporating noncovalent bonds into main-chains. *Adv. Mater.* **32**, 2000096 (2020).
19. R. Schnell, M. Stamm, C. Creton, Direct correlation between interfacial width and adhesion in glassy polymers. *Macromolecules* **31**, 2284–2292 (1998).
20. R. Schnell, M. Stamm, C. Creton, Mechanical properties of homopolymer interfaces: Transition from simple pullout to crazing with increasing interfacial width. *Macromolecules* **32**, 3420–3425 (1999).
21. S. Bode, M. Enke, R. K. Bose, F. H. Schacher, S. J. Garcia, S. van der Zwaag, M. D. Hager, U. S. Schubert, Correlation between scratch healing and rheological behavior for terpyridine complex based metallopolymers. *J. Mater. Chem. A* **3**, 22145–22153 (2015).
22. S. Bode, M. Enke, M. Hernandez, R. K. Bose, A. M. Grande, S. van der Zwaag, U. S. Schubert, S. J. Garcia, M. D. Hager, Characterization of self-healing polymers: From macroscopic healing tests to the molecular mechanism, in *Self-healing Materials*, M. Hager, S. van der Zwaag, U. S. Schubert, Eds. (Advances in Polymer Science, Springer International Publishing, Cham, ed. 4, 2015), vol. 273, pp. 113–142.
23. M. Enke, R. K. Bose, S. Bode, J. Vitz, F. H. Schacher, S. J. Garcia, S. van der Zwaag, M. D. Hager, U. S. Schubert, A metal salt dependent self-healing response in supramolecular block copolymers. *Macromolecules* **49**, 8418–8429 (2016).
24. J. Sautaux, L. Montero de Espinosa, S. Balog, C. Weder, Multistimuli, multiresponsive fully supramolecular orthogonally bound polymer networks. *Macromolecules* **51**, 5867–5874 (2018).
25. S. Bode, L. Zedler, F. H. Schacher, B. Dietzek, M. Schmitt, J. Popp, M. D. Hager, U. S. Schubert, Self-healing polymer coatings based on crosslinked metallosupramolecular copolymers. *Adv. Mater.* **25**, 1634–1638 (2013).
26. A. M. Grande, S. J. Garcia, S. van der Zwaag, On the interfacial healing of a supramolecular elastomer. *Polymer* **56**, 435–442 (2015).
27. A. M. Grande, J. C. Bijleveld, S. J. Garcia, S. van der Zwaag, A combined fracture mechanical–rheological study to separate the contributions of hydrogen bonds and disulphide linkages to the healing of poly(urea-urethane) networks. *Polymer* **96**, 26–34 (2016).
28. A. M. Grande, R. Martin, I. Odriozola, S. van der Zwaag, S. J. Garcia, Effect of the polymer structure on the viscoelastic and interfacial healing behaviour of poly(urea-urethane) networks containing aromatic disulphides. *Eur. Polym. J.* **97**, 120–128 (2017).
29. L. Zedler, M. D. Hager, U. S. Schubert, M. J. Harrington, M. Schmitt, J. Popp, B. Dietzek, Monitoring the chemistry of self-healing by vibrational spectroscopy–Current state and perspectives. *Mater. Today* **17**, 57–69 (2014).
30. S. Kupfer, L. Zedler, J. Guthmuller, S. Bode, M. D. Hager, U. S. Schubert, J. Popp, S. Gräfe, B. Dietzek, Self-healing mechanism of metallopolymers investigated by QM/MM simulations and Raman spectroscopy. *Phys. Chem. Chem. Phys.* **16**, 12422–12432 (2014).
31. M. W. Urban, D. Davydovich, Y. Yang, T. Demir, Y. Zhang, L. Casabianca, Key-and-lock commodity self-healing copolymers. *Science* **362**, 220–225 (2018).
32. C. C. Hornat, M. W. Urban, Entropy and interfacial energy driven self-healable polymers. *Nat. Commun.* **11**, 1028 (2020).
33. H. M. van der Kooij, A. Susa, S. J. García, S. van der Zwaag, J. Sprakel, Imaging the molecular motions of autonomous repair in a self-healing polymer. *Adv. Mater.* **29**, 1701017 (2017).
34. J. R. Kumpfer, J. J. Wie, J. P. Swanson, F. L. Beyer, M. E. Mackay, S. J. Rowan, Influence of metal ion and polymer core on the melt rheology of metallosupramolecular films. *Macromolecules* **45**, 473–480 (2012).
35. D. W. R. Balkenende, S. Coulibaly, S. Balog, Y. C. Simon, G. L. Fiore, C. Weder, Mechanochemistry with metallosupramolecular polymers. *J. Am. Chem. Soc.* **136**, 10493–10498 (2014).
36. L. N. Neumann, I. Gunkel, A. Barron, E. Oveisi, A. Petzold, T. Thurn-Albrecht, S. Schrettl, C. Weder, Structure-property relationships of microphase-separated metallosupramolecular polymers. *Macromolecules* **53**, 5068–5084 (2020).
37. C. Piguet, J.-C. G. Bünzli, G. Bernardinelli, C. G. Bochet, P. Froidevaux, Design of luminescent building blocks for supramolecular triple-helical lanthanide complexes. *J. Chem. Soc. Dalton Trans.* **29**, 83–97 (1995).
38. A. Escande, L. Guénée, K.-L. Buchwalder, C. Piguet, Complexation of trivalent lanthanides with planar tridentate aromatic ligands tuned by counteranions and steric constraints. *Inorg. Chem.* **48**, 1132–1147 (2009).
39. J. B. Beck, S. J. Rowan, Multistimuli, multiresponsive metallo-supramolecular polymers. *J. Am. Chem. Soc.* **125**, 13922–13923 (2003).
40. M. Martínez-Calvo, O. Kotova, M. E. Möbius, A. P. Bell, T. McCabe, J. J. Boland, T. Gunnlaugsson, Healable luminescent self-assembly supramolecular metallogels possessing lanthanide (Eu/Tb) dependent rheological and morphological properties. *J. Am. Chem. Soc.* **137**, 1983–1992 (2015).
41. B. Yang, H. Zhang, H. Peng, Y. Xu, B. Wu, W. Weng, L. Li, Self-healing metallo-supramolecular polymers from a ligand macromolecule synthesized via copper-catalyzed azide–alkyne cycloaddition and thiol–ene double "click" reactions. *Polym. Chem.* **5**, 1945–1953 (2014).
42. L. N. Neumann, C. Calvino, Y. C. Simon, S. Schrettl, C. Weder, Solid-state sensors based on $Eu3^{+}$-containing supramolecular polymers with luminescence colour switching capability. *Dalton Trans.* **47**, 14184–14188 (2018).
43. R. K. Bose, N. Hohlbein, S. J. Garcia, A. M. Schmidt, S. van der Zwaag, Connecting supramolecular bond lifetime and network mobility for scratch healing in poly(butyl acrylate) ionomers containing sodium, zinc and cobalt. *Phys. Chem. Chem. Phys.* **17**, 1697–1704 (2015).
44. T. Yan, K. Schröter, F. Herbst, W. H. Binder, T. Thurn-Albrecht, Unveiling the molecular mechanism of self-healing in a telechelic, supramolecular polymer network. *Sci. Rep.* **6**, 32356 (2016).
45. K. E. Feldman, M. J. Kade, E. W. Meijer, C. J. Hawker, E. J. Kramer, Model transient networks from strongly hydrogen-bonded polymers. *Macromolecules* **42**, 9072–9081 (2009).
46. F. Herbst, S. Seiffert, W. H. Binder, Dynamic supramolecular poly(isobutylene)s for self-healing materials. *Polym. Chem.* **3**, 3084–3092 (2012).
47. T. Rossow, A. Habicht, S. Seiffert, Relaxation and dynamics in transient polymer model networks. *Macromolecules* **47**, 6473–6482 (2014).
48. Z. Ali, K. E. S. Meysam, Asadilman, B. Aydin, B. Yashar, Finite element method analysis of stress intensity factor in different edge crack positions and predicting their correlation using neural network method. *Res. J. Recent Sci.* **3**, 69–73 (2014).
49. A. Susa, R. K. Bose, A. M. Grande, S. van der Zwaag, S. J. Garcia, Effect of the dianhydride/branched diamine ratio on the architecture and room temperature healing behavior of polyetherimides. *ACS Appl. Mater. Interfaces* **8**, 34068–34079 (2016).
50. S. Petoud, J.-C. G. Bünzli, F. Renaud, C. Piguet, K. J. Schenk, G. Hopfgartner, Stability and size-discriminating effects in mononuclear lanthanide triple-helical building blocks with tridentate aromatic ligands. *Inorg. Chem.* **36**, 5750–5760 (1997).
51. R. Dobrawa, P. Ballester, C. R. Saha-Möller, F. Würthner, *Metal-Containing and Metallosupramolecular Polymers and Materials*, U. S. Schubert, G. R. Newkome, I. Manners, Eds. (ACS Symposium Series, American Chemical Society, 2009), vol. 928, pp. 43–62.
52. C. A. García-Franco, B. A. Harrington, D. J. Lohse, Effect of short-chain branching on the rheology of polyolefins. *Macromolecules* **39**, 2710–2717 (2006).

53. S. Tang, A. Habicht, S. Li, S. Seiffert, B. D. Olsen, Self-diffusion of associating star-shaped polymers. *Macromolecules* **49**, 5599–5608 (2016).
54. P. B. Rapp, A. K. Omar, B. R. Silverman, Z.-G. Wang, D. A. Tirrell, Mechanisms of diffusion in associative polymer networks: Evidence for chain hopping. *J. Am. Chem. Soc.* **140**, 14185–14194 (2018).
55. J. Ramirez, T. J. Dursch, B. D. Olsen, A molecular explanation for anomalous diffusion in supramolecular polymer networks. *Macromolecules* **51**, 2517–2525 (2018).

Acknowledgments: We thank I. Gunkel and S. Balog for the help with the SAXS measurements, B. Wilts for the help with some of the preliminary data acquisition by scanning electron microscopy, C. Vallotton and D. Laub for the help with the sample preparation for STEM-EDX analysis, and F. Marx and H. Traeger for the assistance with the preparation of metallopolymer films. **Funding:** The research leading to these results has received funding through the National Center of Competence in Research Bio-Inspired Materials (51NF40-182881), a research instrument of the Swiss National Science Foundation, and the Adolphe Merkle Foundation. **Author contributions:** L.N.N., S.S., and C.W. developed the original concept for the study and designed the materials and experiments. L.N.N. synthesized and characterized the materials and performed the experiments. E.O. performed the STEM experiments with EDX spectroscopy. R.S. helped with the analysis of fracture mechanics measurements. A.P. and T.T.-A. helped with carrying out and analyzing the rheology experiments. All authors discussed the results and contributed to the interpretation of the data. L.N.N., S.S., and C.W. wrote the paper. All authors contributed to editing of the manuscript. **Competing interests:** The authors declare that they have no competing interests. **Data and materials availability:** All data needed to evaluate the conclusions in the paper are present in the paper and/or the Supplementary Materials. The datasets generated during the current study are available from the corresponding authors on reasonable request.

Submitted 20 August 2020
Accepted 10 March 2021
Published 28 April 2021
10.1126/sciadv.abe4154

Citation: L. N. Neumann, E. Oveisi, A. Petzold, R. Style, T. Thurn-Albrecht, C. Weder, S. Schrettl, Dynamics and healing behavior of metallosupramolecular polymers. *Sci. Adv.* **7**, eabe4154 (2021).

Science Advances

Dynamics and healing behavior of metallosupramolecular polymers

Laura N. Neumann, Emad Oveisi, Albrecht Petzold, Robert W. Style, Thomas Thurn-Albrecht, Christoph Weder and Stephen Schrettl

Sci Adv **7** (18), eabe4154.
DOI: 10.1126/sciadv.abe4154

Science Advances (ISSN 2375-2548) is published by the American Association for the Advancement of Science, 1200 New York Avenue NW, Washington, DC 20005. The title *Science Advances* is a registered trademark of AAAS.